Nondestructive inspection of tree trunks using a dual-polarized ground-penetrating radar system

Nondestructive Inspection of Tree Trunks Using a Dual-polarised Ground-Penetrating Radar System

Lilong Zou, *Member, IEEE,* Fabio Tosti, Senior *Member, IEEE*, and Amir M. Alani

***Abstract*— In recent years, trees in European countries have been increasingly endangered by emerging infectious diseases (EIDs). In the United Kingdom, this has been observed to affect whole woodlands and forests, threatening the existence of some types of trees. Although quarantine measures have been taken to limit the spreading of such diseases, this has not yet been effectively controlled leading to millions of trees affected by EIDs. Ground-penetrating radar (GPR) has proven effective in identifying critical features on diseased trees for detection of EIDs spread. However, the irregular shape of tree trunks and their complex internal structure represent real challenges for conventional GPR measurements and signal processing methodologies. In this research, a dual-polarised GPR system is used to detect internal decay in tree trunks using novel signal processing methodologies. A polarisation correlation filter based on Bragg Scattering on a 3D Pauli feature vector and an arc-shaped Kirchhoff migration are discussed in detail. The proposed polarisation correlation filter is utilised to enhance the signal-to-noise ratio (SNR) of B-scans due to bark and tree trunk high-loss properties of tree trunks. Meanwhile, an arc-shaped Kirchhoff migration algorithm is performed to counteract the influence of the bark irregularity. The proposed data processing framework is successfully validated with measurements on a real tree trunk, where cross-sections were subsequently cut for comparison purposes. Outcomes from the proposed methodology demonstrate a high consistency with the features observed on the tree trunk cross-sections, indicating the reliability of the proposed detection scheme for assessing tree-decay associated with EIDs.**

***Index Terms*— ground-penetrating radar (GPR), dual-polarised radar; non-destructive testing (NDT); decay inspection; tree trunk; emerging infectious diseases (EIDs)**

I. Introduction

In recent years, an increase throughout pests and diseases has harmed trees in Europe, particularly in the United Kingdom (UK). Multiple types of virus, often known as emerging infectious diseases (EIDs), have infected whole forests and woods. EIDs are being more recognised as a global risk to human development, including climate change and food security. Plant diseases continue to pose a hazard as current knowledge progresses. In reality, EIDs spread has been accelerated by commerce and transportation, as well as the capacity of microbes to adapt the changing surroundings as a result of climate change [1]. The consequences can be severe, since diseases are on the rise and might lead to the loss of more fragile tree species. In both the UK and the United States (US), EIDs have turned into the abolition of approximately 100 million elm trees. 3.5 billion chestnut trees in the US died from chestnut blight [2]. Between 2000 and 2020, the loss of EIDs-infected pine trees has resulted in the emission of at least 270 megatons of CO_2 in Western Canada, at a large economic cost to both the carbon released and the wood. Prevalence of EIDs on trees has substantially affected the ecological variety, requiring extensive management and huge losses of fixed CO_2. EIDs spread the fungus through a special beetle of the bark that targets leaves and branches [3]-[5]. This causes the tree to become starving and progressively die. Because predictive modelling and small-scale studies will never be able to completely predict disease spread and severity in the future, intensive monitoring and surveillance are increasingly required. Aside from enhanced monitoring, it is critical to integrate theoretical and practical epidemiology, climatic projections, genomic surveillance, and molecular evolution monitoring to develop clear and urgent EIDs control techniques for effective preventive and timely control [6][7]. Moreover, estimating tree trunk structure accurately is critical for preventing tree collapses in urban areas or near roadways.

As a result, monitoring and controlling EIDs is a difficult and vital undertaking. In addition to preventing its spread, it is critical to be able to quickly diagnose tree disease at an early stage and treat it effectively. On the other hand, early indicators of tree disease are often present in the tree inner core which making it difficult to spot particular signs of illness on the tree exterior surface. In view of the above, detecting decay in living trees is certainly a challenging task. Simple approaches, which are still commonly used right now, are based on the experience of operators, such as determining the existence of attenuation by making trees sound. However, these basic methods can only determine whether the tree is diseased or not and are generally unable to obtain more comprehensive details. Other destructive methods, such as core drilling techniques, can be used to determine the internal structure of trees. However, living trees cannot be subjected to damaging inspections such as core

Manuscript received xx xx, xxxx; revised xx xx, xxxx; accepted xx xx, xxxx. *(Corresponding author: Lilong Zou.)*

Lilong Zou, Fabio Tosti and Amir M. Alani are with the School of Computing and Engineering, University of West London, W5 5RF London, UK (e-mail: lilong.zou@uwl.ac.uk; fabio.tosti@uwl.ac.uk; amil.alani@uwl.ac.uk).

drilling or, in the worst-case scenario, tree chopping down. Moreover, these approaches are time-consuming and laborious to introduce. At the same time, they can cause permanent harm to the tree itself, rendering the tree more vulnerable to disease. More importantly, these approaches can only provide information at the sampling point and cannot monitor the overall disease status and evolution of the entire tree.

In that sense, nondestructive testing (NDT) has been introduced as a solution for assessing the internal structure of tree trunk. NDT techniques such as electrical resistivity tomography, ultrasound tomography, infrared thermography, X-ray computed tomography and neutron imaging have been used for tree trunk inspection [8]. As a recognised NDT technology, Ground penetrating radar (GPR) is becoming more widely used in environmental engineering [9]-[14]. GPR is a real-time NDT technology that generates high-resolution data in a short amount of time using high-frequency electromagnetic (EM) waves. This method employs EM waves that propagate at a specified speed dictated by the permittivity of the material. In a word, GPR is a practical alternative because it allows for nondestructive trunk assessment. GPR system can rebuild the internal structure of a live trunk cross-section quite well. However, when it comes to non-destructive tree examination, traditional GPR calculation approaches have its drawbacks. To begin with, living trees contain a lot of water, which makes it difficult for high-frequency EM waves to travel through the trunk. In [15], the relative permittivity is given as 20 to assess the internal structure of a real hollow tree. The radar signal with 2 GHz centre frequency can only penetrated a dozen centimeters into the tree trunk. While a lower frequency system may provide more penetration depth, it is not practicable to use due to system size constraints and resolution requirement. Moreover, unlike the unusual shape of the ground surface, the irregular shape of the tree trunk makes traditional data collection and processing difficult to be performed [16]. Therefore, inspecting the small decay inside the tree trunk is a challenge task.

To overcome the above challenges, a dual-polarised GPR system was employed for non-destructive inspection of a living tree trunk in this paper. In the field of microwave remote sensing, polarisation technology has been one of the most important for the past decades [17]-[19]. It refers to the orientation of the electric field vector, which can be employed by polarimetric radar to characterise target characteristics. Polarimetric decompositions are polarimetric analytic methods that can be used to obtain polarisation-related properties. These methodologies were widely used in polarimetric synthetic aperture radar (SAR) data-based topography and land-use categorization. [20]-[22]. In recent years, polarimetry has been introduced into GPR research to improve its detection capability concurrently with the rapid development of polarisation technology. The attempt to use polarimetric radar systems for subsurface feature inspection starts from 1995 [23]. Following that, polarimetric GPR methods, such as polarimetric borehole radar is developed and signal processing methodologies are applied for detection of subsurface fractures [24]-[27], unexploded ordnance (UXO) [28][29], detection of targets [30]-[32], and linear objects [33]-[35]. Meanwhile, polarimetric analysis methods are applied to improve the capability of GPR for classification of subsurface targets [36][37].

In [38], we have reported a simple approach which trying to combine HH and VV polarimetric GPR profiles together to find out the decays or anomalies for tree trunk inspection. Following that idea, we propose a complete and improved methodology for polarimetric GPR signal processing in this paper. The proposed methodology is different from any existing signal processing algorithms using polarimetric GPR system. The core part is derived from the Bragg Scattering 3D Pauli feature vector. Based on that, a polarisation correlation filter is built with first and second scattering vectors. The working principle of the proposed filter is similar to polarimetric coherence which has widely used in polarimetric remote sensing. The designed filter can both keep the weak reflection and suppress the noise, even if the weak reflection is below the noise level. In the meantime, arc-shaped Kirchhoff migration algorithm is performed to suppress the effect of the irregular shape of the tree trunk. The proposed data processing framework is successfully validated with measurement on a real tree trunk, where cross-sections were subsequently cut for comparison purposes.

This article is organised as follows. Section II described the proposed processing methodologies, including pre-processing, ringing noise removal, polarisation correlation filter, and arc-shaped Kirchhoff migration. In Section III, the real measurement strategy, and results on a living tree are presented. Discussions on results are also conducted. Conclusions follow in Section IV.

II. Processing Methodology

This research uses a four-stage processing pipeline. To raise the total signal to clutter ratio, a pre-processing procedure for time correction and signal noise filtering is first implemented. The ringing noise caused by the multiple layers of the tree trunk is then removed using the singular value decomposition (SVD). After that, the proposed polarisation correlation filter is utilised to improve the signal-to-noise ratio (SNR) of B-scans, which is caused by tree trunk bark and high-loss qualities. Then, the arc-shaped Kirchhoff migration is used in the last stage to mitigate the impact of the irregular shape of the tree trunk. Finally, a 3D image mapping the decay of the tree trunk is created for further interpretation.

A. Pre-processing

After data collection with the dual-polarimetric GPR system, the raw data were formed by a group of B-scans. As a result, data pre-processing processes such as zero-time correction, direct coupling subtraction, and band pass filtering were applied to the acquired raw data. In GPR signal processing, the zero-time correction is used to correct the starting point of the surface reflection. To eliminate the superfluous B-scan antenna coupling between transmitter and receiver, direct coupling subtraction is used. The band pass filter is performed to the initial processing for noise suppression.

B. *Ringing Noise Removal*

A regular tree trunk is made up of five layers: bark, phloem, cambium, heartwood, and sapwood. In terms of water content, chemical makeup, and texture, each of these levels is presents distinctive features. This produces dielectric differences, resulting in recurrent reflections and, as a result, an overall ringing noise.

In B-scan outputs, ringing noise behaves similarly. This is why ringing noise is often reduced by simple averaging removal in common GPR surveys. However, averaging removal does not work well in tree inspection due to the irregular shape of the tree trunk. Ringing noise does not show a constant arrival time in the B-scan. In difficult settings with variable surface conditions, SVD could provide a more precise and systematic solution to minimise ringing noise.

Specifically, a factorisation of the form $U\Sigma V^*$ is the SVD of a $m\times n$ complex matrix M. The matrix U is a $m\times m$ complex unitary matrix. Σ is a rectangular diagonal matrix with non-negative real integers on the diagonal of size $m\times n$. V is a $n\times n$ dimensional complex unitary matrix.

In any singular value decomposition, the following condition applies:

$$M = U\Sigma V^* \tag{1}$$

where the singular values of M are equivalent to the diagonal elements of Σ. Large eigenvalues are linked to dominating repeated features, which are most commonly connected with ringing noise. In the case of tree inspections, ringing noise shows the dominant feature for horizontal events. Five dominating eigenvalues in matrix Σ are set to zero and a new matrix $\overline{\Sigma}$ is obtained based on the rebuild B-scan qualities. Then, the new B-scan $\overline{M}$ after removing ringing noise is formed as follows:

$$\overline{M} = U\overline{\Sigma}V^*. \tag{2}$$

C. *Polarisation Correlation Filter*

On polarimetric SAR data, the information content of backscattering polarimetric signatures has been explored against the effect of surface roughness over the last few years [39][40]. In GPR investigations, reflections from targets can be assumed as a Bragg Scattering in the working frequency at a certain incidence. Most of the electromagnetic (EM) wave energy is incident on the target surface covered by waves of small slope and a backscattered signal is produced by the component of the reflected wave.

Cloude and Papathanassiou give a complete generic formulation for polarimetric radar [22]. Each channel dataset is measured by fully polarimetric radar devices using a 2×2 complicated scattering matrix. To generalise spatial coherence, a coherent scattering vector k can be recovered by vectorizing the scattering matrix [21]. In a monostatic backscattering scenario, the reciprocity constrains the sinclair scattering matrix to be symmetrical, that is, $\overline{M}_{HV} = \overline{M}_{VH}$. As a result, the four-dimensional polarimetric target vectors are reduced to three-dimensional polarimetric target vectors. The scattering vector for the monostatic situation can be obtained using Pauli basis matrices as [17]:

$$k = \begin{bmatrix} \overline{M}_{HH} + \overline{M}_{VV} \\ \overline{M}_{HH} - \overline{M}_{VV} \\ 2\overline{M}_{HV} \end{bmatrix}. \tag{3}$$

It can be supposed that there is only one dominant eigenvector for Bragg scattering (depolarisation is insignificant), and that the eigenvector is given by:

$$k = \begin{bmatrix} \overline{M}_{HH} + \overline{M}_{VV} \\ \overline{M}_{HH} - \overline{M}_{VV} \\ 0 \end{bmatrix}. \tag{4}$$

In GPR electromagnetics, changes in permittivity difference and target geometry affect the EM reflection. Furthermore, the polarisation of the transmitting and receiving antenna, as well as the shape and electrical properties of the scatterers, have a significant impact on the received EM back reflection from subsurface structures. The electric and magnetic fields of GPR EM waves are transverse to the propagation direction, making them vectors in nature. For the identification of discontinuities, approaches that combine both polarisation invariant information and waveform information into a single, clearly interpretable attribute reflection are preferred.

The first component $\left(\overline{M}_{HH} + \overline{M}_{VV}\right)$ of the scattering vector in (4) enhance much more the reflection information from the target body and contribute to suppress the decorrelated noise level. The coherent noise generated by the system, etc. is much reduced in the second component $\left(\overline{M}_{HH} - \overline{M}_{VV}\right)$ of the scattering vector in (4). Therefore, a polarisation correlation filter based on the first and second components of the scattering vector is proposed as:

$$PCF = \frac{\left|\overline{M}_{HH} + \overline{M}_{VV}\right|^2 - \left|\overline{M}_{HH} - \overline{M}_{VV}\right|^2}{\sqrt{\left|\overline{M}_{HH} + \overline{M}_{VV}\right| \cdot \left|\overline{M}_{HH} - \overline{M}_{VV}\right|}}. \tag{5}$$

In (5), the denominator has the function of normalising the numerator term and avoid extreme value. The working principle of the proposed filter is similar to correlation. If a mathematical expansion of the numerator in (5) is performed, only the cross term $\overline{M}_{HH} \cdot \overline{M}_{VV}$ will be preserved. This cross term has the similar form with the polarimetric coherence term:

$$C = \frac{\left\langle \overline{M}_{HH} \cdot \overline{M}_{VV}^* \right\rangle}{\sqrt{\left\langle \left|\overline{M}_{HH}\right| \right\rangle^2} \sqrt{\left\langle \left|\overline{M}_{VV}\right| \right\rangle^2}}. \tag{6}$$

The expectation value is denoted by $\langle \ldots \rangle$ and $*$ denotes the complex conjugate. The coherence magnitude is defined from 0 to 1. It measures the degree of the correlation between HH and VV channels and with 1 denoting perfect correlation. While the polarimetric coherence cannot directly apply to the GPR B-scan, because it is not complete imaged data. In that case, we proposed the polarisation correlation filter (as shown in (5)) which can strengthen the correlation between HH and VV GPR measurements. It can be very effective in suppressing noise, recovering and strengthening the useful signals that below the noise level. More importantly, it maintains the signal phase

information which represents the target time delay in the GPR measurement.

D. *Arc-shape Kirchhoff Migration*

To reconstruct the 3D inner structure of the inspected tree trunk, 3D migration algorithm has been performed on the processed data. 3D Kirchhoff migration is the process that attempts to overcome this problem by geometrically re-locating targets in the subsurface and time back into their true subsurface position. Kirchhoff migration process can be time-consuming and expensive in case outputs with a relatively high-resolution are required.

In this paper, we have proposed an arc-shape Kirchhoff migration approach based on an optimal imaging aperture. The imaging aperture is selected based its equivalent diameter and the GPR system antenna radiation pattern, as α described in (7). The arc-shape Kirchhoff migration has low computational and operational requirements, making it ideal for large-scale forestry applications. As described in Fig. 1, the imaging resolution is composed of an azimuth angle $d\theta$, a radial resolution dr and a vertical resolution dz .

Mathematically, the output wave field $I(z_{out},\theta_{out},r,t)$ of tree trunk after Kirchhoff migration is obtained by solving the scalar wave equation from the wave field with zero offset $PCF(z_{in},\theta_{in},r_{surface},t)$, which corresponding to (5) in the above subsection. The zero offset data is measured at the surface of tree trunk. The comprehensive migration solution is provided by:

$$I(z_{out},\theta_{out},r,t)=\frac{1}{2\pi}\iint\left[\frac{\cos\alpha}{R^2}PCF\left(z_{in},\theta_{in},r_{surface},t+\frac{R}{v}\right)+\frac{\cos\alpha}{vR}\frac{\partial}{\partial t}PCF\left(z_{in},\theta_{in},r_{surface},t+\frac{R}{v}\right)\right]dzd\theta \quad (7)$$

where v is the RMS velocity. R is the path from the target point (z_{out},θ_{out},r) to the observation point $(z_{in},\theta_{in},r_{surface})$ at tree trunk surface. α is the angle of incident wave relating to the antenna radiation pattern.

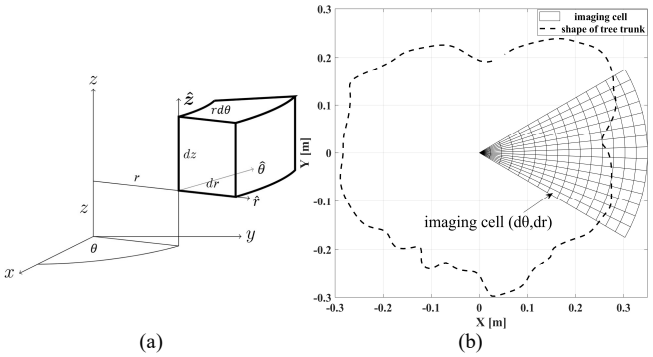

(a) (b)

Fig. 1. Illustration of the arc-shape Kirchhoff migration setup; (a) cylindrical coordinate system; (b) arc imaging cell.

III. Measurement Results and Discussion

A. *Survey site and Strategy*

The field inspection measurement is performed on a live horse chestnut tree at Kensington Gardens - The Royal Parks, London, United Kingdom, as shown in Fig. 2 (a). Considering the health condition of the leaves at the inspection period, we could roughly diagnose that the tree was suffering disease. The height of the tree was about 20 m and the radius of the tree trunk is approximately 30 cm.

Survey the tree trunk of every 5 cm along the main axis of the tree and parallel to the ground and circular scans were obtained. The entire scanned area is 1.5 m long and comprises of 30 parallel circular scans, as illustrated by the red circle in Fig.2 (b). The investigated region has a variable circumference and a pseudo-cylindrical form. The circumference of each piece was accurately estimated and then included into the detecting procedure using the measuring-wheel device affixed to the antenna. Meanwhile, 8 vertical scans were performed from top to bottom on the investigated volume, as shown by the black lines in Fig.2 (b).

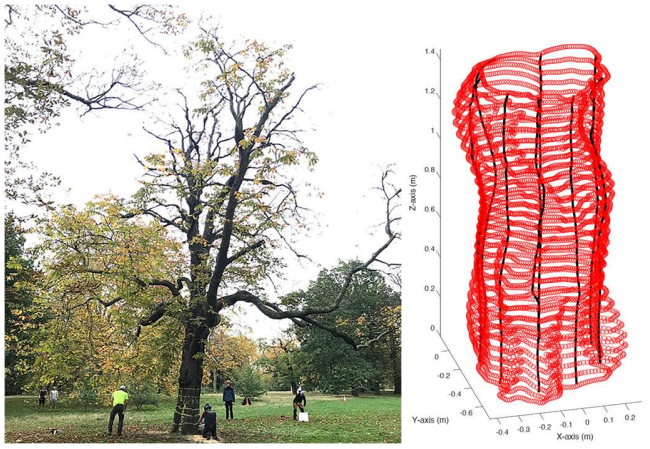

(a) (b)

Fig. 2. (a) The horse chestnut tree under investigation at Kensington Gardens – The Royal Parks, London, UK; (b) The survey lines of measurements on the investigated tree. Red dotted lines indicate the transverse circular measurements. Black lines along the *z*-axis indicate the longitudinal measurements.

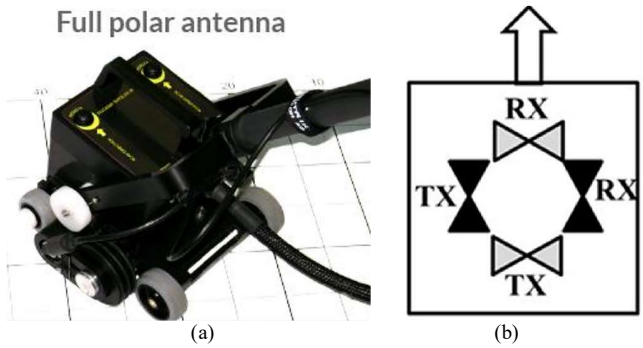

(a) (b)

Fig. 3. The dual-polarized system for tree inspection; (a) Aladdin system; (b) antenna configuration.

B. *Dual-polarised GPR System*

This study employs the compact dual polarised "Aladdin" GPR system, which is a product of IDS GeoRadar (part of Hexagon), as shown in Fig.3 (a). The system has two 2GHz antennas that are polarised perpendicular to one another (HH

and VV channels), allowing for simultaneous acquisition of polarimetric data [41]. The antenna configuration was shown in Fig. 3 (b). Deeper surveying is possible due to the dual polarisation, which allows for views of shallow and deep structures.

C. *Results and Discussion*

For a healthy tree, the water content inside the trunk is more evenly distributed and gradually increasing from the bark to the inside. The moisture content of living trees is in fact between 35% and 60% [42]. This means that if there is decay or a hollow in the middle of the trunk, there will be a significant change in its dielectric constant, which indicates a fundamental change in the structure at the boundary of healthy wood.

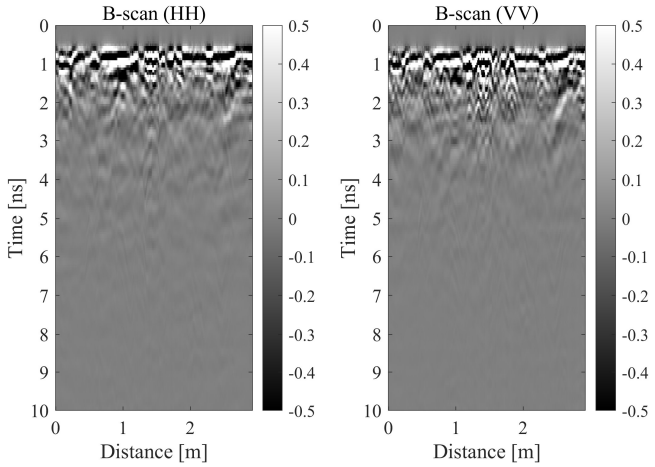

Fig. 4. HH and VV B-scan after implementation of pre-processing steps.

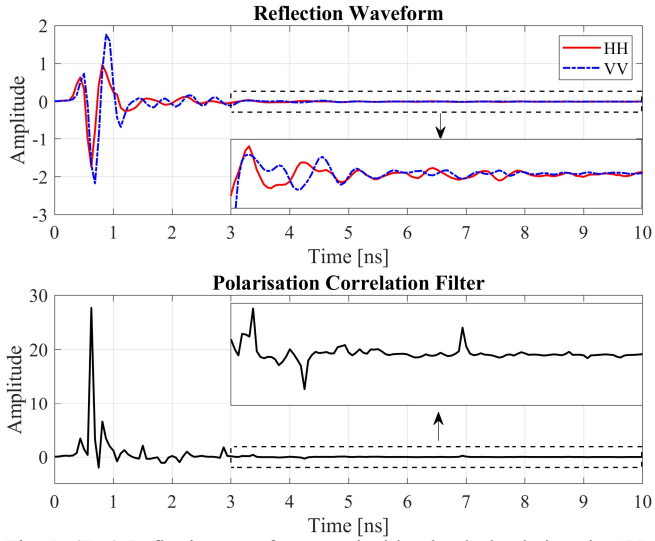

Fig. 5. (Top) Reflection waveform acquired by the dual-polarimetric GPR system (HH and VV) and (Bottom) the reconstructed waveform after the application of the polarisation correlation filter.

Using the proposed signal processing procedures, representative results are showed and discussed in this section. Fig. 4 shows a B-scan of HH and VV components after pre-processing. In the GPR profile, relatively clear reflections can be observed from 0 to 3 ns. Reflection signals become weaker after 3 ns. This is due to the fact that the tree trunk is fully saturated with water, as the horse chestnut tree is still alive. The data quality deteriorates in a tree with moist decay within, and the signal-to-noise ratio approaches one. This can be explained by reflection losses near the boundary of decayed zone, according to EM wave theory. Conduction currents due to excessive moisture content, as well as scattering due to inhomogeneous structure. In other words, low data quality is the primary problem of trunk detection with GPR.

In Fig.5, the top figure shows the reflection waveform of HH and VV components. As it shown in the enlarged window in the figure, the reflection cannot be distinguished from the noise. The bottom figure in Fig. 5 shows the result after the proposed polarisation correlation filter. As we can see from the corresponding enlarged window, the SNR of the reconstructed waveform has greatly improved. At the meantime, the filtered results kept the signal phase which represent the time delay from the anomies inside the tree trunk. The B-scan generated by using the suggested polarisation correlation filter is shown in Fig. 6. Compared to Fig.4, the reflected signal after 3 ns can be clearly observed.

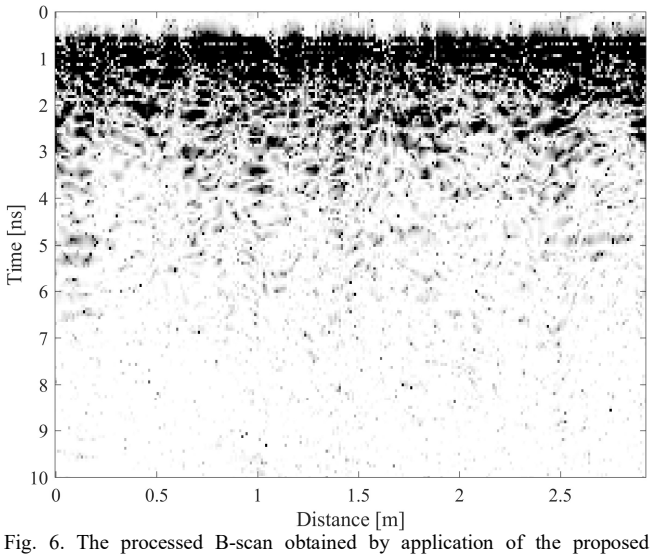

Fig. 6. The processed B-scan obtained by application of the proposed polarimetric correlation filter.

According to the moisture content of the tree trunk, the relative permittivity ε_r is given as 28 to reconstruct the 3D images when apply the proposed arc-shape Kirchhoff migration algorithm. After the measurements were completed, the tree was chopped down (as shown in Fig. 2 (a)) and split into multiple slices to reveal its internal structure. One of reconstructed sections at the bottom of the investigated tree trunk is shown in Fig. 7 (a). The high energy parts indicate the anomalies matching the decay inside the trunk. In the central area of the achieved image, an irregular low energy shape can be observed (white dashed line). Compared to the corresponding real cross-section in Fig. 7 (b), we can conclude that the irregular pattern matches the boundary of the hollow which having a diameter of about 20 centimetres.

Figure 8 (a) and (b) show the reconstructed section at the top

of the investigated tree trunk and the corresponding cut section, respectively. A prominent decline extending down the main axis of the cross-section can be seen in Fig. 8 (b). The decay has an irregular shape and a strong transition between the healthy sapwood and the decayed sapwood. The high energy parts in Fig. 8 (a) match with the visible decay very well. The white dashed line in Fig. 8 (a) tracking the low-energy area indicates the hollow perimeter internal to the cross-section. The widest part of the hollow is approximately 10 cm long.

A prospective view of the resulting 3D image of the trunk are shown in Fig.9 (a) and (c), while the corresponding real picture are shown in Fig.9 (b) and (d). From Fig. 9 (a), a major feature can be seen extending from the bottom of the trunk throughout – approximately – the full height of the investigated volume. This is in good agreement with the tree true structure, as illustrated in Fig. 9 (b). The shape and size of decays are reconstructed correctly. Looking at the 3D image reconstruction from a different prospect view, as shown in Fig.9 (c), relatively good conditions can be diagnosed for the trunk. This also matches with the true internal structure of tree as seen in Fig. 9. (d). According to the results, dual-polarised GPR systems combined with the proposed strategy can correctly identify concealed decays in a time- and cost-effective way.

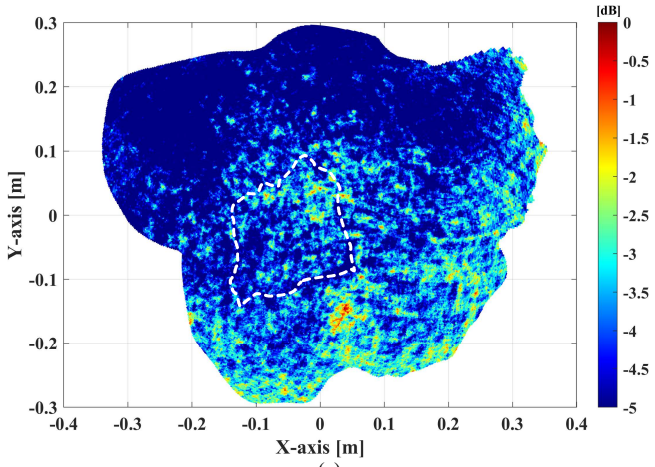

(a)

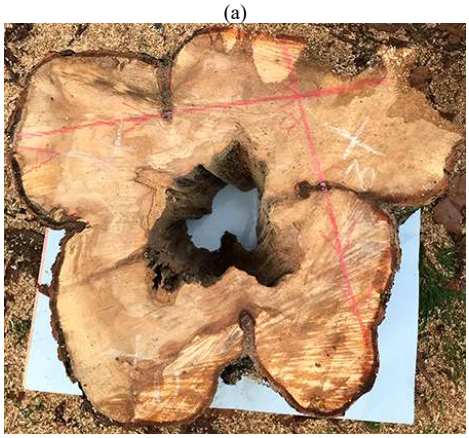

(b)

Fig. 7. Polarimetric reconstruction of one of the investigated tree trunk sections; (a) reconstruction by the proposed approach, where the internal white dashed line indicates the hollow boundary; (b) corresponding section of the horse chestnut tree.

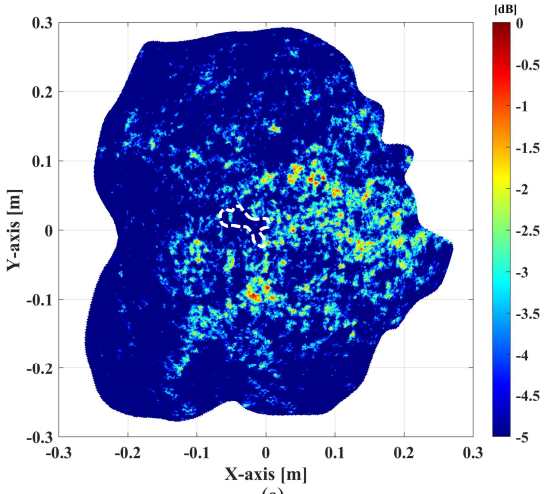

(a)

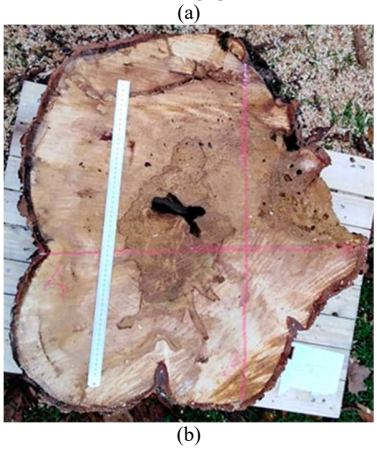

(b)

Fig. 8. Polarimetric reconstructions of the investigated tree trunk sections; (a) reconstructions by proposed approach, where white line indicate the hollow boundary; (b) corresponding section of the horse chestnut tree.

IV. Conclusion

A new processing framework in unhealthy trees for identifying concealed deterioration and cavities is presented using a dual-polarized ground penetrating radar (GPR) is presented in this paper. The proposed methodology has proven effective at clearly and accurately detecting decay in a living tree. The scheme of processing pipeline is made up primarily of a pre-processing step, a singular value decomposition (SVD), a polarisation correlation filter and an arc-shape Kirchhoff migration algorithm. To enhance the signal-to-noise ratio (SNR) of B-scans produced by the bark and high-loss qualities of tree trunks, a polarisation correlation filter is proposed based on a 3D Pauli feature vector of Bragg Scattering. The arc-shape Kirchhoff migration technology has low computing and operational requirements, making it especially interesting for large-scale forestry applications. It also reduces the effect of the irregular shape effect of tree trunk. The accuracy of the proposed framework is tested against real-life cross-section features. Comparison demonstrates a high consistency between predicted and actual conditions indicating the reliability of the proposed detection scheme for detecting tree-decay associated with emerging infectious diseases (EIDs).

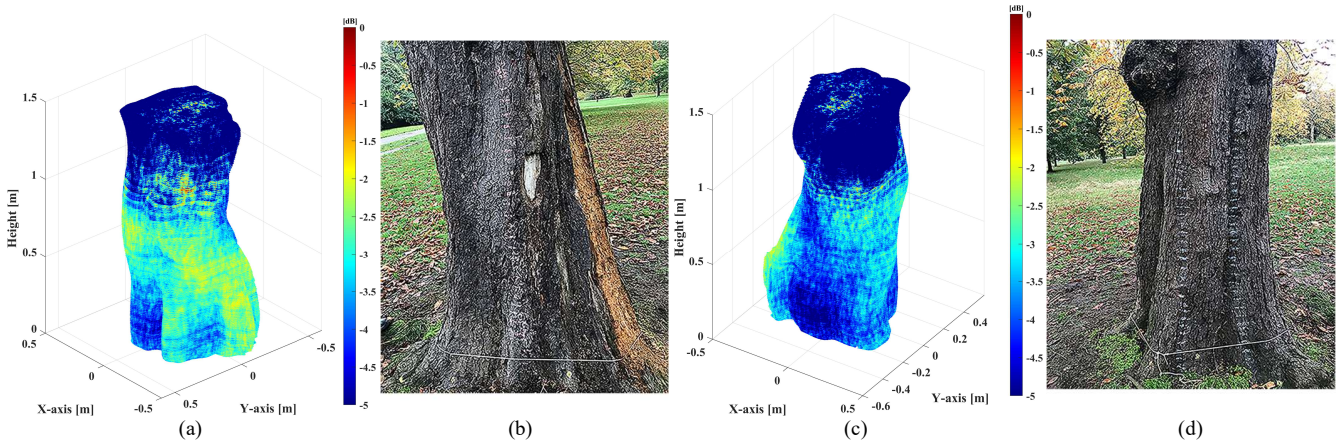

Fig. 9. The reconstructed internal structure of the scanned area using the proposed processing scheme; (a) 3D reconstructed image view from one side; (b) the corresponding trunk view of (a) on site; (c) 3D reconstructed image view from another side; (d) the corresponding trunk view of (c) on site.

ACKNOWLEDGMENTS

This research was funded by the following trusts, charities, organisations and individuals for their generosity in supporting this project: Lord Faringdon Charitable Trust, The Schroder Foundation, Cazenove Charitable Trust, Ernest Cook Trust, Sir Henry Keswick, Ian Bond, P. F. Charitable Trust, Prospect Investment Management Limited, The Adrian Swire Charitable Trust, The John Swire 1989 Charitable Trust, The Sackler Trust, The Tanlaw Foundation, and The Wyfold Charitable Trust. The authors would like to express their sincere thanks to Kensington Gardens – The Royal Parks, London, UK for facilitating this research.

REFERENCES

[1] M. C. Fisher, A. D. Henk, C. J. Briggs, J. S. Brownstein, L. C. Madoff, S. H. McCraw and S. J. Gurr, "Emerging fungal threats to animal, plants and ecosystems," *Nature*, vol. 484, pp. 186–194, Apr. 2012.

[2] W. C. Shortle, K. R. Dudzik, *Wood Decay in Living and Dead Trees: A Pictorial Overview*, U.S. Forest Service, 2012.

[3] L. V. McKinnery, L. R. Nielsen, D. B. Collinge, I. M. Thomsen, J. K. Hansen and E. D. Kjaer, "The ash dieback crisis: variation in resistance can prove a long-term solution," *Plant Pathol.*, vol. 63, no.3, pp. 485–499, Jan. 2014.

[4] S. Denman, N. Brown, S. Kirk, M. Jeger and J. Webber, "A description of the symtpoms of Acute Oak Decline in Britain and a comparative review on causes of similar disorders on oak in Europe," *Forestry*, vol. 87, no. 4 pp. 535-551, Oct. 2014.

[5] N. Brown, D. J. G. Inward, M. Jeger and S. Denman, "A review of Agrilus biguttatus in UK forests and its relationship with acute oak decline," *Forestry*, vol. 88, no. 1, pp. 53–63, Jan. 2015.

[6] A. Abbott, "Italy's olive crisis intensifies as deadly tree disease spreads," *Nature*, vol. 563, pp. 306–307, Nov. 2018.

[7] N. Brazee, R. Marra, L. Goecke and P. Van Wassenaer, "Non-destructive assessment of internal decay in three hardwood species of northeastern North America using sonic and electrical impedance tomography," *Forestry*, vol. 84, no.1, pp. 33-39, Jan. 2011.

[8] I. Giannakis, F. Tosti, L. Lantini and A. M. Alani, "Health Monitoring of Tree Trunks Using Ground Penetrating Radar," *IEEE Trans. Geo. Remote Sens.*, vol. 57, no. 10, pp. 8317-8326, Oct. 2019.

[9] A. M. Alani and L. Lantini, "Recent advances in tree root mapping and assessment using non-destructive testing methods: a focus on ground penetrating radar," *Surv. Geophys.*, vol. 41, pp. 605-646, May 2020.

[10] L. Lantini, F. Tosti, I. Giannakis, L. Zou, A. Benedetto and A.M. Alani, "An Enhanced Data Processing Framework for Mapping Tree Root Systems Using Ground Penetrating Radar," *Remote Sens.*, vol. 12, no. 20, pp. 3417, Oct. 2020.

[11] A. Benedetto, F. Tosti, L. B. Ciampoli and F. D'Amico, "GPR applications across engineering and geosciences disciplines in Italy: A review," *IEEE J. Sel. Topics Appl. Earth Observ. Remote Sens.*, vol. 9, no. 7, pp. 2952-2965, Jul. 2016.

[12] J. Jezova, L. Mertens and S. Lambot, "Ground-penetrating radar for observing tree trunks and other cylindrical objects," *Constr. Build. Mater.*, vol. 123, pp. 214–225, Oct. 2016.

[13] L. Zou, L. Yi and M. Sato, "On the Use of Lateral Wave for the Interlayer Debonding Detecting in an Asphalt Airport Pavement Using a Multistatic GPR System," *IEEE Trans. Geo. Remote Sens.*, vol. 58, no. 6, pp. 4215-4224, Jun. 2020.

[14] J. R. Butnor, M. L. Pruyn, D. C. Shaw, M. E. Harmon, A. N. Mucciardi and M. G. Ryn, "Detecting defects in conifers with ground penetrating radar: applications and challenges," *Forest Pathol.*, vol. 39, no.5, pp. 309-322, Oct. 2009.

[15] F. Tosti, G. Gennarelli, L. Lantini, I. Catapano, F. Soldovieri, I. Giannakis, and A.M. Alani, "The use of GPR and microwave tomography for the assessment of the internal structure of hollow trees," *IEEE Trans. Geosci. Remote Sens.*, vol. 60, pp. 1-14, Sep. 2022.

[16] A. M. Alani, I. Giannakis, L. Zou, L. Lantini and F. Tosti, "Reverse-Time Migration for Evaluating the Internal Structure of Tree-Trunks Using Ground-Penetrating Radar," *NDT&E Int.*, vol. 115, pp. 102294, Oct. 2020.

[17] J. J. van Zyl, H. A. Zebker and C. Elachi, "Imaging radar polarimetric signatures: Theory and observation," *Radio Sci.*, vol. 22, no. 4, pp. 529-543, Jan. 1987.

[18] H. Zebker and J. J. Van Zyl, "Imaging radar polarimetry: A review," *Proc. IEEE*, vol. 79, no. 11, pp. 1583-1606, Nov 1991.

[19] W. M. Boerner, W. L. Yan, A. Q. Xi and Y. Yamaguchi, "On the basic principles of radar polarimetry—The target characteristic polarization state theory of Kennaugh Huynen's polarization fork concept and its extension to the partially polarized case", *Proc. IEEE*, vol. 79, pp. 1538-1550, Oct. 1991.

[20] J. S. Lee, M. R. Grunes, T. L. Anisworth, L. Du, D. L. Schuler and S. R. Cloude, "Unsupervised classification using polarimetric decomposition and the complex Whishart classifier," *IEEE Trans. Geosci. Remote Sens.*, vol. 37, no. 5, pp. 2249-2258, Sep. 1999.

[21] J. S. Lee, M. R. Grunes and G. De Grandi, "Polarimetric SAR speckle filtering and its impact on terrain classification," *IEEE Trans. Geosci. Remote Sens.*, vol. 37, no. 5, pp. 2363-2373, Sep. 1999.

[22] S. R. Cloude and E. Pottier, "A review of target decomposition theorems in radar polarimetry," *IEEE Trans. Geosci. Remote Sens.*, vol. 34, no. 2, pp. 498-518, Mar. 1996.

[23] M. Sato, T. Ohkubo and H. Niitsuma, "Cross-polarization borehole radar measurements with a slot antenna," *Appl. Geophys.*, vol. 33, no. 13, pp. 53-61, Jan. 1995.

[24] T. Miwa, M. Sato and H. Niitsuma, "Subsurface fracture measurement with polarimetric borehole radar," *IEEE Trans. Geosci. Remote Sens.*, vol. 37, no. 2, pp. 828-837, Mar. 1999.

[25] T. Miwa, M. Sato and H. Niitsuma, "Enhancement of reflected waves in single-hole polarimetric borehole radar measurement," *IEEE Trans. Antennas Propag.*, vol. 48, no. 9, pp. 1430-1437, Sep. 2000.

[26] M. Sato and T. Miwa, “Polarimetric borehole radar system for fracture measurement,” *Subsurf. Sens. Technol. Appl.*, vol. 1, no. 1, pp. 161-174, Jan. 2000.
[27] M. Sato and M. Takeshita, “Estimation of subsurface fracture roughness by polarimetric borehole radar,” *IEICE Trans. Electron.*, vol. E83-C, no. 12, pp. 1881-1888, Dec. 2000.
[28] C. Chen, M. B. Higgins, K. O'Neill and R. Detsch, “Ultrawide-bandwidth fully-polarmetric ground penetrating radar classification of subsurface unexploded ordnance,” *IEEE Trans. Geosci. Remote Sens.*, vol. 39, no. 6, pp. 1221-1230, Jun. 2001.
[29] K. O'Neill, “Discrimination of uxo in soil using broadband polarimetric GPR backscatter,” *IEEE Trans. Geo. Remote Sens.*, vol. 39, no. 2, pp. 356-367, Feb. 2001.
[30] J. Zhao and M. Sato, “Radar polarimetry analysis applied to single-hole fully polarimetric borehole radar,” *IEEE Trans. Geosci. Remote Sens.*, vol. 44, no. 12, pp. 3547-3554, Dec. 2006.
[31] J. Zhao and M. Sato, “Consistency analysis of subsurface fracture characterization using different polarimetry techniques by a borehole radar,” *IEEE Geosci. Remote Sens. Lett.*, vol. 4, no. 3, pp. 359-363, Jul. 2007.
[32] D. S. Sassen and M. E. Everett, “3D polarimetric GPR coherency attributes and full-waveform inversion of transmission data for characterizing fractured rock,” *Geophys.*, vol. 74, no. 3, pp. J23-J34, May/Jun. 2009.
[33] H. Liu, J. Zhao and M. Sato, “A hybrid dual-polarization GPR system for detection of linear objects,” *IEEE Antennas Wireless Propag. Lett.*, vol. 14, pp. 317-320, Oct. 2014.
[34] V. R. N. Santos and F. L. Teixeira, “Study of time-reversal-based signal processing applied to polarimetric GPR detection of elongated targets,” *J. Appl. Geophys.*, vol. 139, pp. 257-268, Apr. 2017.
[35] H. Liu, X. Huang, F. Han, J. Cui, B. F. Spencer and X. Xie, “Hybrid polarimetric GPR calibration and elongated object orientation estimation,” *IEEE J. Sel. Topics Appl. Earth Observ. Remote Sens.*, vol. 12, no. 7, pp. 2080-2087, Jul. 2019.
[36] X. Feng, Y. Yu, C. Liu and M. Fehler, “Combination of H-Alpha decomposition and migration for enhancing subsurface target classification of GPR,” *IEEE Trans. Geosci. Remote Sens.*, vol. 53, no. 9, pp. 4852-4861, Sep. 2015.
[37] Z. Dong, X. Feng, H. Zhou, C. Liu and M. Sato, "Effects of induced field rotation from rough surface on H-Alpha decomposition of full-polarimetric GPR", *IEEE Trans. Geosci. Remote Sens.*, vol. 59, no. 11, pp. 9192-9208, Nov. 2021.
[38] L. Zou, L. Lantini, F. Tosti and A.M. Alani, "Tree trunk inspections using a polarimetric GPR system." *SPIE in Earth Resources and Environmental Remote Sensing/GIS Applications XII*, vol. 11863, pp. 192-195, Sep. 2021.
[39] F. Mattia, T. Le Toan, J. C. Souyris, G. De Carolis, N. Floury, F. Posa, et al., “The effect of surface roughness on multifrequency polarimetric SAR data,” *IEEE Trans. Geosci. Remote Sens.*, vol. 35, no. 4, pp. 954-966, Jul. 1997.
[40] I. Hajnsek, E. Pottier and S. R. Cloude, “Inversion of surface parameters from polarimetric SAR,” *IEEE Trans. Geosci. Remote Sens.*, vol. 41, no. 4, pp. 727-744, Apr. 2003.
[41] F. Lombardi, M. Lualdi, F. Picetti, P. Bestagini, G. Janszen and L.A. Di Landro, "Ballistic Ground Penetrating Radar Equipment for Blast-Exposed Security Applications", *Remote Sens.*, vol. 12, no. 4, pp. 717, Jan. 2020.
[42] C.M. Stewart, "Moisture content of living trees", *Nature*, vol. 214, no. 5084, pp. 138-140, Apr. 1967.